Physica Scripta

PAPER • OPEN ACCESS

Spectroscopic study for the role of polymer binding agent in the quasi-harmonic field emission behavior of polymer graphite field emission cathodes

To cite this article: Mohammad M Allaham *et al* 2025 *Phys. Scr.* **100** 035977

IOP Publishing Phys. Scr. 100 (2025) 035977 https://doi.org/10.1088/1402-4896/adb704

Physica Scripta

RECEIVED
5 September 2024

REVISED
29 January 2025

ACCEPTED FOR PUBLICATION
17 February 2025

PUBLISHED
26 February 2025

PAPER

Spectroscopic study for the role of polymer binding agent in the quasi-harmonic field emission behavior of polymer graphite field emission cathodes

Mohammad M Allaham[1,2,3], **Samer I Daradkeh**[1,3], **Zuzana Košelová**[2,4], **Rashid Dallaev**[3], **Dinara Sobola**[1,3,5] **and Alexandr Knápek**[2,4]

[1] Central European Institute of Technology, Brno University of Technology, Brno 61264, Czech Republic
[2] Institute of Scientific Instruments of Czech Academy of Sciences, Brno 61200, Czech Republic
[3] Department of Physics, Faculty of Electrical Engineering and Communication, Brno University of Technology, Brno 610101, Czech Republic
[4] Department of Microelectronics, Faculty of Electrical Engineering and Communication, Brno University of Technology, Brno 61200, Czech Republic
[5] Institute of Physics of Materials, Czech Academy of Sciences, Brno 61662, Czech Republic

E-mail: allaham@vutbr.cz

Keywords: polymer graphite, colloidal graphite, current-Raman spectroscopy, quasi-harmonic field emission, Raman spectroscopy

Supplementary material for this article is available online

Abstract

Graphite-based microcathodes have shown significant performance when operated as cold field emission electron sources. Specifically mentioned, cathodes that have been prepared from highly ordered pyrolytic graphite and polymer graphite pencil leads. Such cathodes are characterized by low operating voltages, a long lifetime, a cheap fabrication price, and a stable emission current. Recently, it was shown that polymer graphite cold field emission cathodes have a unique quasi-harmonic field emission behavior, where the process included emission of pulses of electrons with relatively higher emission current values. However, this behavior has not been reported for other graphite-based materials. In this paper, we study the effects of the polymer binding agent on the charge carriers' flow through the surface of polymer graphite using Raman-current spectroscopy. The results from polymer graphite were then compared to cathodes prepared from colloidal graphite conductive paint when deposited on a glass substrate. The results showed that the $I(D)/I(G)$ ratio of polymer graphite had a fluctuating behavior, which was not the case for colloidal graphite, which had a more stable structure.

1. Introduction

Recent development of graphite-based electrodes and cold field emission cathodes showed that this type of electron source has several beneficial advantages, such as a long lifetime, lower operating voltages, high emission current densities, stable emission currents, and lower vacuum conditions of operation [1–4]. Among the graphite-based materials, conductive polymer graphite electrodes have been under study for the past few years because of their simple and cheap fabrication methods. Polymer graphite (or pencil graphite) is a conductive graphitic rod that is formed by binding graphite microflakes using an elastic non-ceramic polymer-based binding agent. The fabrication process is usually performed in an oxygen-free atmosphere [5–8].

In recent studies, the cold field emission behavior of polymer graphite cathodes (PGC) was characterized with unique pulses of emitted electrons. These pulses appeared in the current-time characteristics as sudden peaks in the recorded spectra. Moreover, these peaks were clearly visible after the tip of the PGC was coated with a single component epoxy resin, which led to the conclusion that the polymer material within the structure of the PGC was behind this phenomenon due to the charging and discharging effects. The appearance of such peaks was recorded and described by Knápek *et al* as a quasi-harmonic emission of electrons with emission current values higher than the average emission current as presented in figure 1 [9].

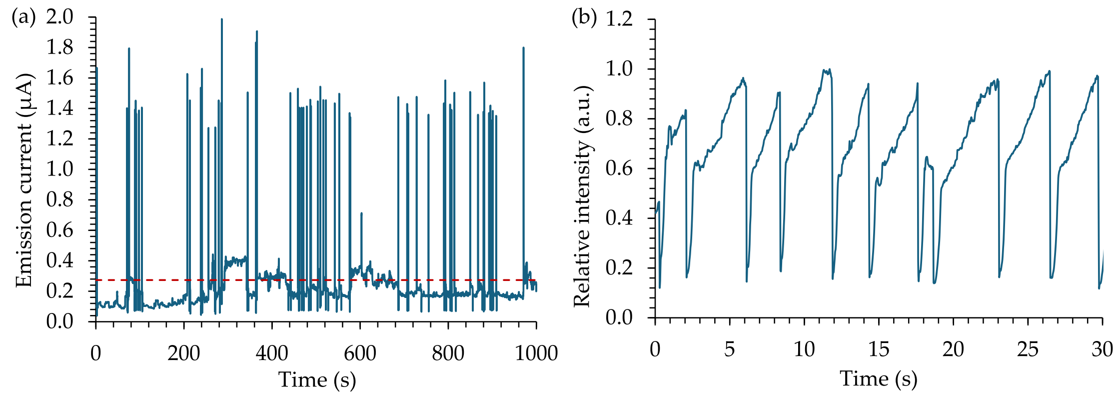

Figure 1. Field emission quasi-harmonic behavior of a polymer graphite cathode when operated at 2.7 kV. (a) presents the current-time characteristics, and (b) presents the relative beam intensity (for more details please check [9]).

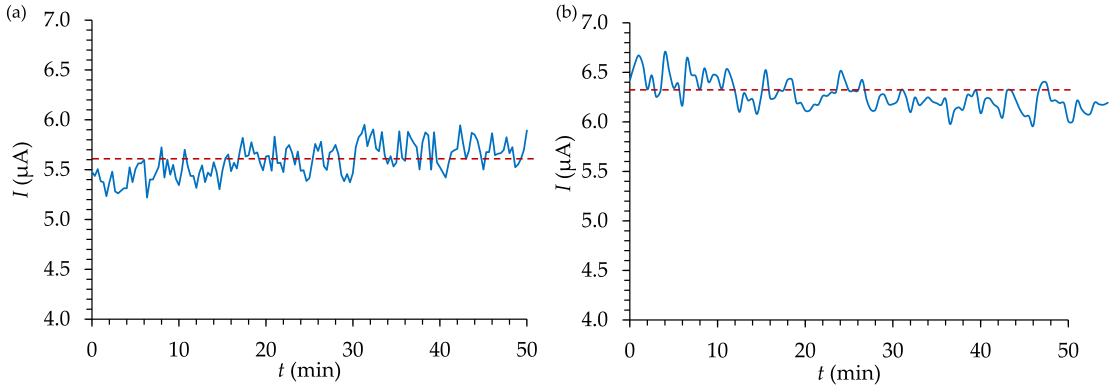

Figure 2. Cold field emission current-time characteristics from colloidal graphite of two glass-graphite samples. Here (a) is for the first sample with average emission current of 5.6 μA and (b) is for the second sample with average emission current of 6.3 μA (for more details please check [10]).

The peaks in figure 1(a) present the electron pulses emitted as appeared in the current-time characteristics that show the fluctuations of the emission current. Moreover, figure 1(b) shows the relative intensity of the field emission pattern over time, which was recorded during the emission process and analyzed over time. The phenomenon of quasi-harmonic pulses has not been reported earlier in the literature of cold emission of electrons. Moreover, a recent study on an almost similar type of cold field emission cathode reported stable and higher emission currents from colloidal graphite microflakes deposited on glass microtips. As shown in figures 2(a and b) for two different samples, the emission current is more stable over time without producing periodic high intensity peaks [10].

In this paper, we study possible structural reasons behind the quasi-harmonic behavior of PGCs. This was done by investigating the vibrational states of the chemical bonds in the cathode structure during the flow of charge carriers. For this purpose, Raman spectroscopy of the PGC surface will be studied while the sample is connected to a simple electrical circuit. The Raman shift spectra were measured at different current-voltage values, and the ratios between the defects and the graphite peaks were reported to understand this behavior.

The results of PGCs were then compared with the results obtained from pure graphite films, which were obtained by coating glass substrate rods with colloidal (conductive) graphite paint. The colloidal graphite films were fabricated by dissolving the graphite microflakes in isopropanol alcohol, resulting in homogeneous graphite films. Moreover, reflected electron energy loss spectroscopy (REELS) was measured for polymer and colloidal graphite samples. The resulting spectra were then compared with the HOPG REELS spectrum, which was used as a reference sample to study the plasmon-electron interaction energies in polymer and colloidal graphite [11–13].

2. Materials and methodology

2.1. Materials

Polymer graphite pencil leads (H, 0.5 mm) from the KOH-I-NOOR HARDTMUTH company (České Budějovice, Czech Republic) were used in this study. This type of polymer graphite has been subjected to several

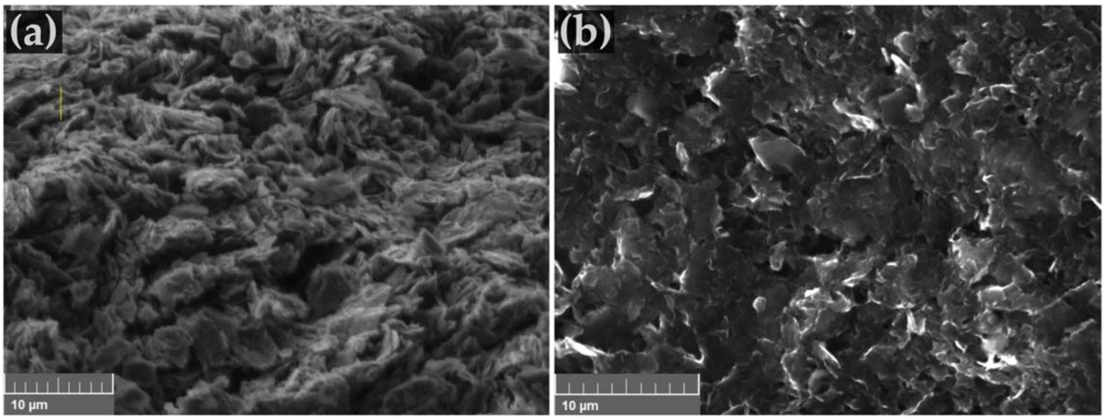

Figure 3. Scanning electron micrographs showing the surface of (a) polymer graphite and (b) colloidal graphite.

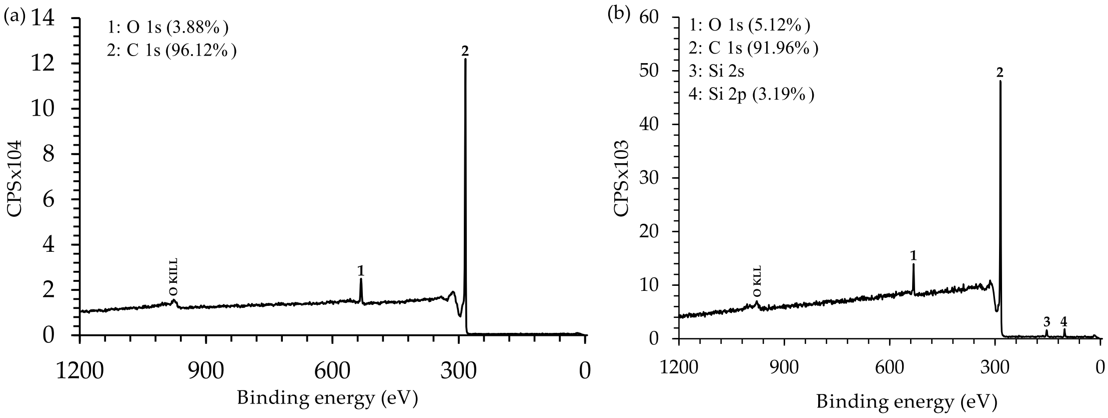

Figure 4. The XPS spectra for (a) graphite conductive paint, and (b) polymer graphite.

studies of different research interests related to its electrochemical applications, scanning probe performance, and cold field emission applications [4, 5, 9, 14–17]. According to the safety data sheet, these pencil leads are manufactured from graphite microflakes, clays ($Al_2Si_2O_5(OH)_4$), and waxes (hydrocarbon polymers). In addition, Industries Europe (Zele, Belgium) KONTAKT CHEMIE graphite 33 conductive paint was used as a source of pure graphite cathodes by coating glass tubes of 2mm in diameter with graphite liquid. Scanning electron micrographs for a polymer graphite surface are presented in figure 3(a), while figure 3(b) shows the surface of colloidal graphite when deposited on glass.

To compare the surface chemical composition of the two materials, we used the AXIS Supra TM x-ray photoelectron spectrometer to obtain the XPS spectra from the polymer graphite cathodes (PGCs) and colloidal graphite cathodes (CGCs). The results are shown in figure 4(a) for colloidal graphite and in figure 4(b) for polymer graphite. The results show a higher purity in the case of colloidal graphite that contained 96.12% of carbon and 3.88% of oxygen, while polymer graphite contained 91.96% of carbon, 5.12% of oxygen, and 3.18% of silicon. The presence of silicon on the surface of polymer graphite is related to the existence of clays in the binding agent used to fabricate polymer graphite pencil leads [18, 19].

In addition, XPS images for $250 \times 500\ \mu m^2$ were obtained from each sample and presented in figure 5. The distribution and intensity of each element described its contribution to the flow of electrical current. It is important to checkthe distribution of silicon in each case, where in the case of CGC it was observed with very low intensity, meaning that it was detected from the glass substrate and, thus, it is related to structural defects in the graphite layer. However, in the case of PGC, it was observed at different intensities, showing that it would have a significant role as a defect impurity.

According to the XPS results, the colloidal graphite samples should have more stable flow of the electrical currents because the electrical contact between the graphite flakes of the CGCs is not interrupted by the presence of any binding agent.

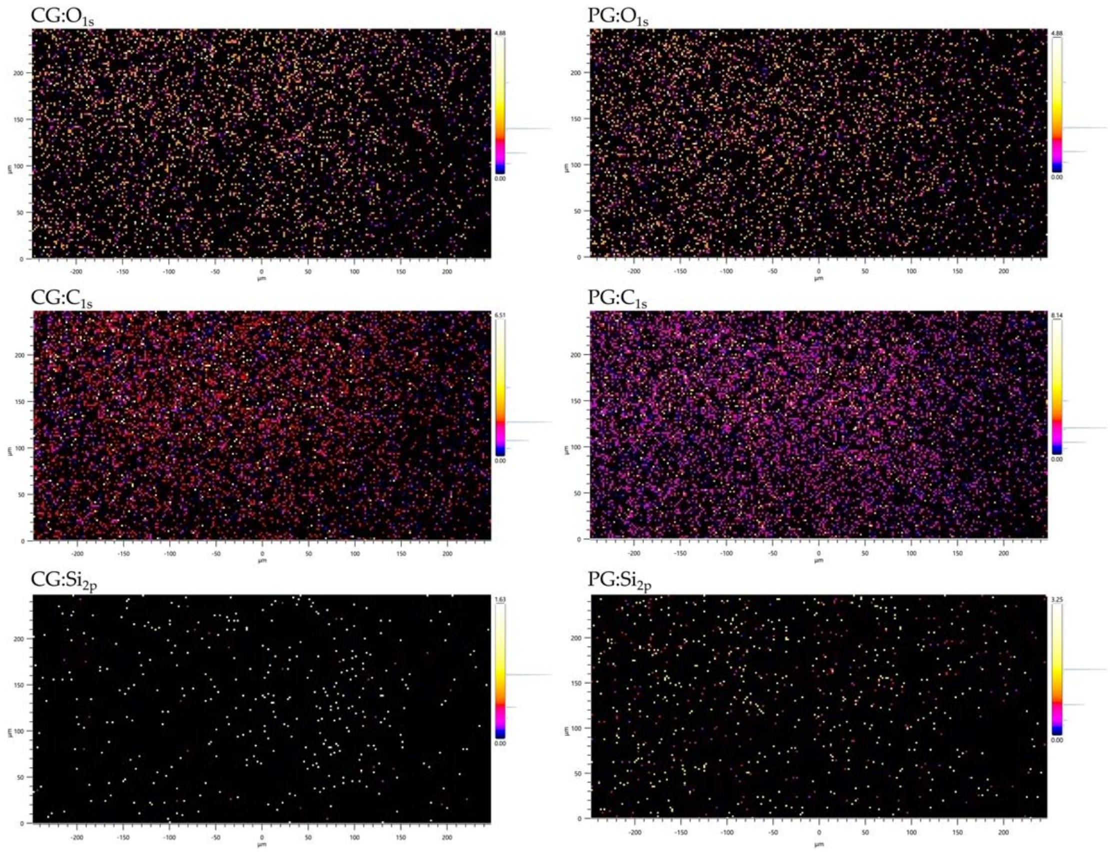

Figure 5. The XPS imaging for a 250 × 500 μm^2 area describing the intensity of elements for collidal graphite on glass (CG) and polymer graphite (PG).

2.2. Methodology

WITec confocal Raman imaging system alpha300 R was used to obtain the Raman shift spectra. A green laser of 532 nm excitation wavelength and 10 mW of laser power was used. Furthermore, a Zeiss EC Epiplan-Neofluar objective lens of 10X magnification power was used to focus the laser beam on the surface of the sample. To ensure precise and significantly acquired statistical results, the spectra were acquired with 10 s as the integration time and 10 accumulations for each scan.

The Raman shift was obtained while the electrical current flows through the tested sample. The sample was connected to a simple DC circuit of variable voltage supply as presented in figure 6. Moreover, the Raman spectroscopy results were supported by studying the REELS spectra of both materials compared to those of HOPG. The results were obtained using the same instrumentation as XPS, with a 1 keV electron beam.

3. Results and discussion

To study the stability of the surface structure during the flow of the electrical current, Raman spectroscopy analyses were obtained for the PGC and CGC samples. Studying the vibration behavior of the surface chemical bonds at different electrical current values provides beneficial information about surface stability.

Starting with the PGC, its normalized Raman spectra are presented in figure 7 for six current values (0–5 mA). For simple peak marking, the fitted peaks in the first defect peak (main defect tone) were denoted by D_n and the fitted peaks in the second defect (overtone) were denoted by $2D_n$. Here, n is the number of the peak as it appeared in the corresponding spectrum. Note that n replaces the (’,”,...) marking method of the defect peaks in the literature. In addition, the figures were normalized by setting the envelope at the G peak as the reference peak. Thus, the intensity of the G peak is not fixed at 1, which is important to include its behavior in the study. Furthermore, since the G peak describes the in-plane vibrations of the C-C bond in graphitic structures, the behavior of the G peak during the current flow describes the importance of the lattice arrangements for the charge carriers flowing through the surface of graphitic electrodes.

According to figure 7(a), the fitted peaks appeared at the following ($1/\lambda$, intensity) pairs before closing the circuit (0 mA current): the $sp^2 - sp^3$ carbon bonds at (1232.77 cm^{-1}, 0.042), first defects peak D_1 at (1346.54 cm^{-1}, 0.300),

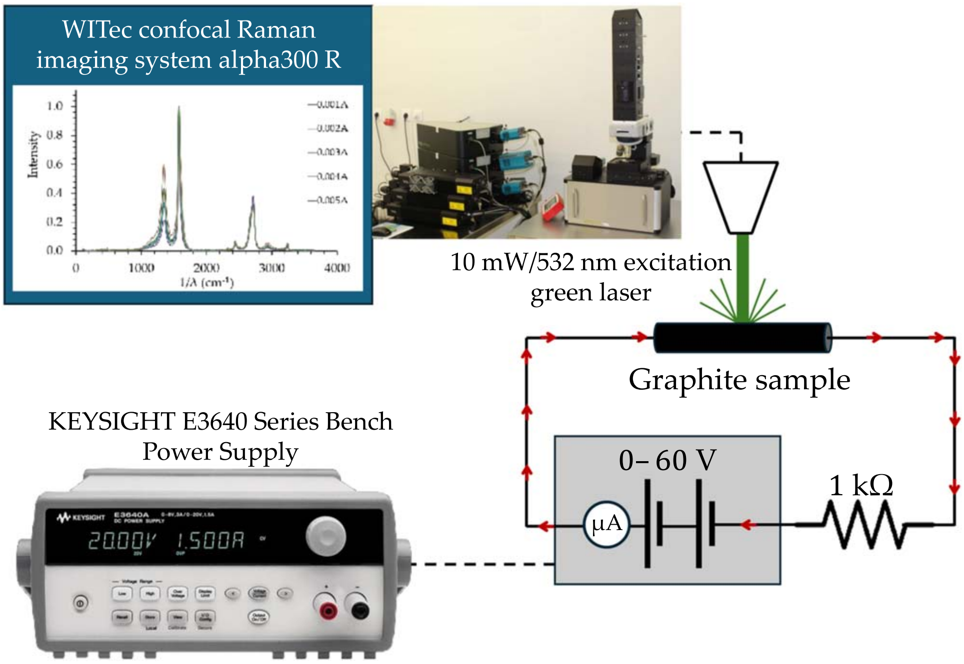

Figure 6. The Raman-current spectroscopy setup.

graphitic bonds G at (1575.63 cm^{-1}, 0.963), second peak of the first defects D_2 at (1616.25 cm^{-1}, 0.150), first overtone peak $2D_1$ at (2691.19 cm^{-1}, 0.279), and second overtone peak $2D_2$ at (2718.6 cm^{-1}, 0.097). These sets of data are used as reference values to study the changes in the peaks information at different current values.

The next step was to measure the Raman spectrum at each current value in the range 1–9 mA. For simplicity, the Raman spectra are presented in figures 7(b)–(f) for current values 1–5 mA. However, Supplemental table 1 shows more detailed results for the full current range (please check the supplementary materials for the attached Supplemental tables 1–4). At 1 mA, the Raman spectrum is presented in figure 7(b) and following the data presented in the Supplemental table 1, the peak $sp^2 - sp^3$ was found at 1212.15 cm^{-1} with intensity of 0.040, reporting a shift of -20.62 cm^{-1} in the peak wavenumber (the minus sign indicates a shift to a lower wavenumber) and a reduction of 7.03% in its intensity. The peak D_1 was shifted by -2.36 cm^{-1} to a wavenumber of 1344.18 cm^{-1}, and the intensity increased by 31.93% reaching 0.396. The G peak was shifted by $+1.45$ cm^{-1} to a wavenumber of 1577.08 cm^{-1}, and its intensity decreased by 4.42% to 0.920. The peak D_2 was shifted by -4.57 cm^{-1} to a wavenumber of 1611.69 cm^{-1}, and its intensity increased by 65.55% to 0.248. In addition, the peak $2D_1$ appeared at 2696.01 cm^{-1} reporting a shift of $+4.82$ cm^{-1}, and its intensity increased by 0.07% to 0.280. However, the $2D_2$ peak reported a shift of $+2.56$ cm^{-1} to a wavenumber of 2721.16 cm^{-1}, and its intensity increased by 4.15% to 0.102.

Moreover, considering $I(D) = I(D_1) + I(D_2)$, its value reports an increase in the $I(D)/I(G)$ ratio from 46.78% to 70.05%. According to this information, the structural and impurity defects increased when the electrical circuit was closed because of the electrical current flow.

The Raman spectra obtained for the current values 2–5 mA are presented in figures 7(c)–(f). For this interval, new peaks appeared within the first defect peak, which are the D_3 and D_4 peaks. The peak analyzes are summarized in Supplemental table 1, in addition to the analysis results obtained from the current interval 6–9 mA. The D_3 peak appeared at a wavenumber of 1350.41 cm^{-1} when the current was 2 mA. It had a shift of $+12.50$ cm^{-1} to a wavenumber of 1362.91 cm^{-1} when the current increased to 3 mA and towards lower wavenumbers until 1351.55 cm^{-1} when the current value was 6 mA, reporting its absence after increasing the current value to 7 mA. The peak D_4 also appeared starting from the current value of 2 mA. However, its peak wavenumber and intensity fluctuated to higher and lower values, and it was noticed at all current values starting from 2 mA.

It is also noted that the intensity of the G peak fluctuated, where its maximum was reported at a current of 4 mA (0.992) and its minimum was at a current of 6 mA (0.858). Moreover, the defects peak had its minimum intensities when the current value was 4 mA, indicating the maximum surface graphitic structure and the most enhanced current flow when the current was 4 mA.

To present these changes, the intensities of the peaksare presented in figure 8(a) as a function of the flowing current. Moreover, the $I(D)/I(G)$ ratio was measured from the intensities of the D_1 peak, along with the $I(\Sigma D)/I(G)$ and $I(\Sigma 2D)/I(G)$ ratios, where ΣD presents the sum of all the peak intensities of the first defects, and $\Sigma 2D$ represents the summation of the intensities of the overtone peaks. The results are summarized in the

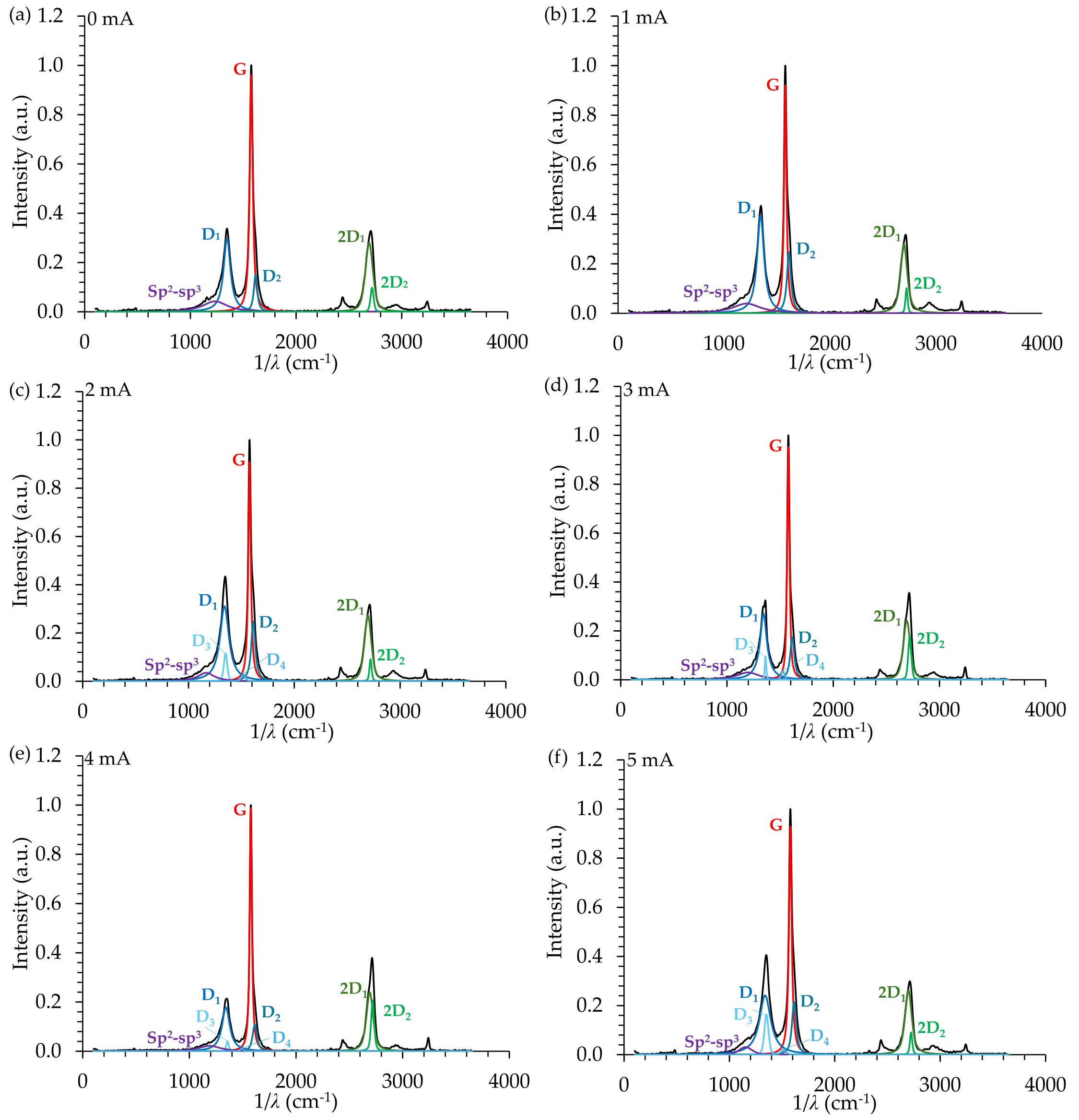

Figure 7. Raman spectroscopy analysis of polymer graphite when an electrical current of (a) 0 mA, (b) 1 mA, (c) 2 mA, (d) 3 mA, (e) 4 mA, and (f) 5 mA is flowing the sample surface.

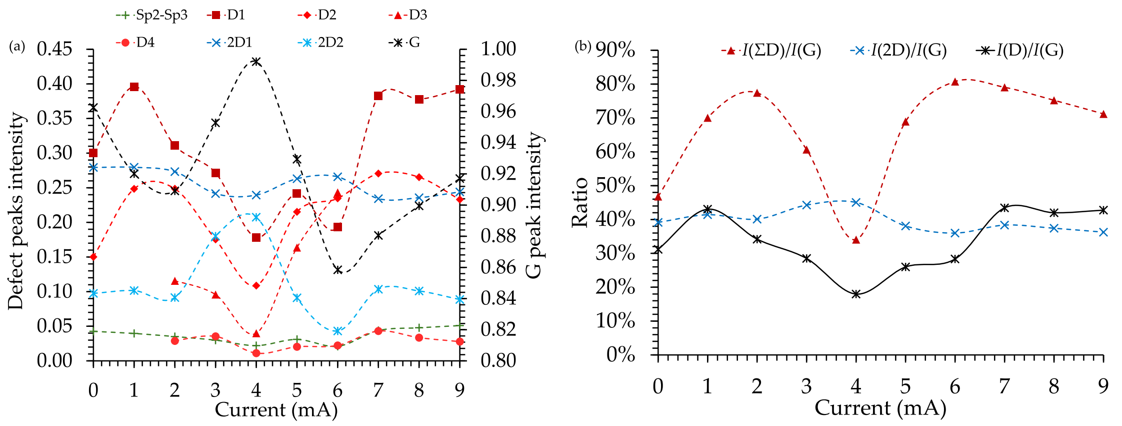

Figure 8. The changes in Raman shift (a) peaks intensity and (b) defects to graphitic intensity ratio as functions of the flowing electrical current.

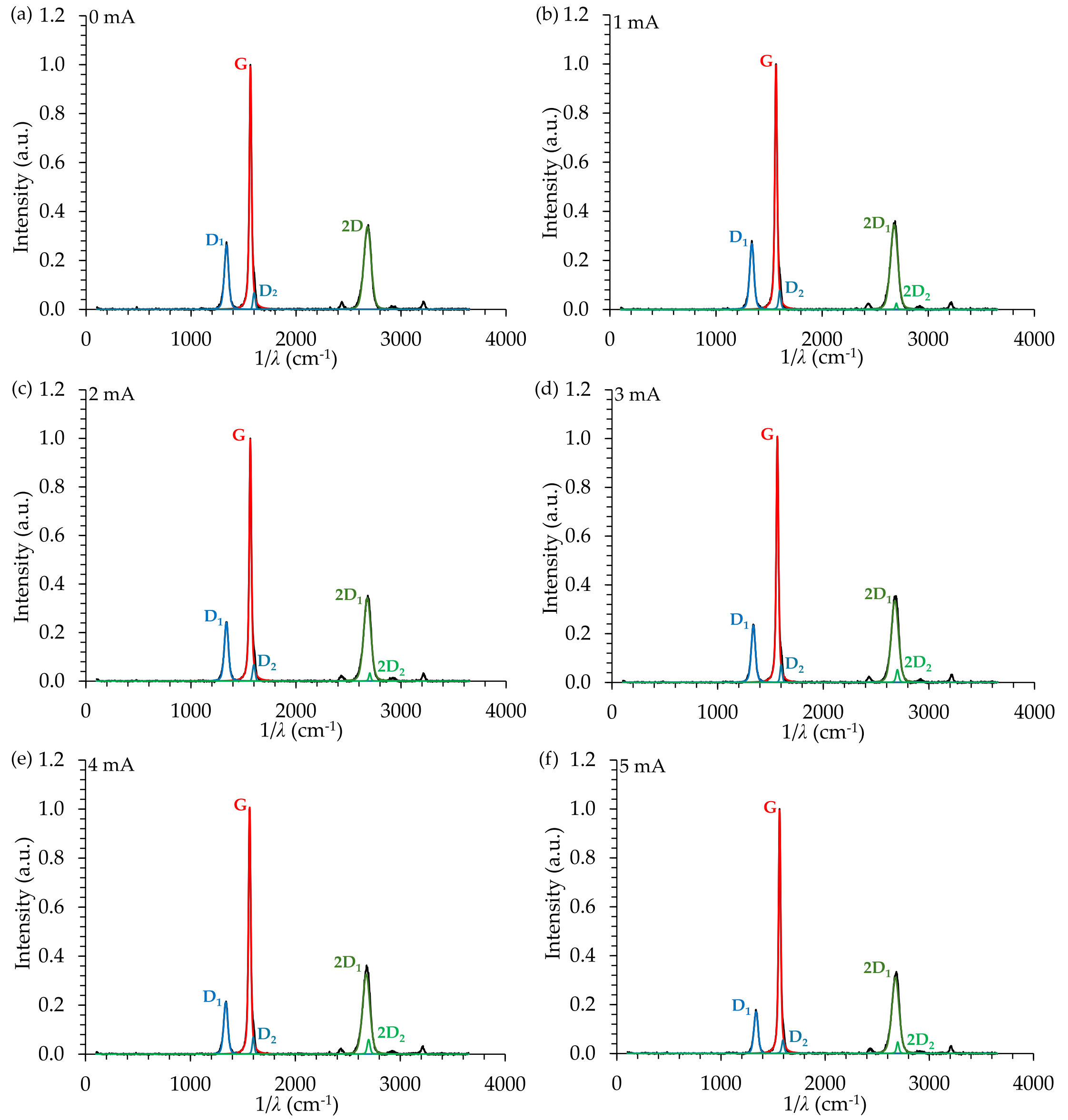

Figure 9. Raman spectroscopy analysis of graphite conductive paint when an electrical current of (a) 0 mA, (b) 1 mA, (c) 2 mA, (d) 3 mA, (e) 4 mA, and (f) 5 mA is passing the sample.

Supplemental table 2 and presented in figure 8(b). The results show that the minimum $I(\mathrm{D})/I(\mathrm{G})$ (17.977%) and $I(\Sigma\mathrm{D})/I(\mathrm{G})$ (34.073%) were reported at 4 mA, in addition to a quasi-harmonic behavior for all the measured ratios.

To investigate the effect of impurities and the amorphous graphite structure on the current flow through PGCs, Raman spectra were collected from the CGC, and the resulted spectra were compared to what was obtained from the PGC. As presented in figure 2(a), the GCP sample consisted mainly of graphite. Thus, investigating the effects of surface vibrations should provide more details on the impact of impurities and defects on current flow through CGC. The results of Raman spectroscopy are presented in figure 9 for current values 0–5 mA. Moreover, the peak analyses are presented in the supplemental table 3.

Before closing the circuit, the results showed the defect peaks D_1 and D_2, the $2\mathrm{D}_1$ overtone, along with the G peak. After closing the circuit, the G peak was almost stable with an increase in intensity from 0.995–0.997 as in figure 10(a). However, its position did not have significant changes until the current value was 4 mA, reporting a change from 1565.730 cm^{-1} to 1564.389 cm^{-1}, which was followed by another shift to 1562.551 cm^{-1} at 5 mA. Regarding the peak D_1, its intensity increased after closing the circuit from 0.269 to 0.339 at 1 mA, but then decreased as the current increased reaching an intensity of 0.171 at 5 mA. Changes in peak intensity are presented as a function of flowing current and presented in figure 10(a). In addition, the ratios $I(\mathrm{D})/I(\mathrm{G})$, $I(\Sigma\mathrm{D})/I(\mathrm{G})$, $I(\Sigma 2\mathrm{D})/I(\mathrm{G})$ are presented in figure 10, where the results showed a continuous improvement in

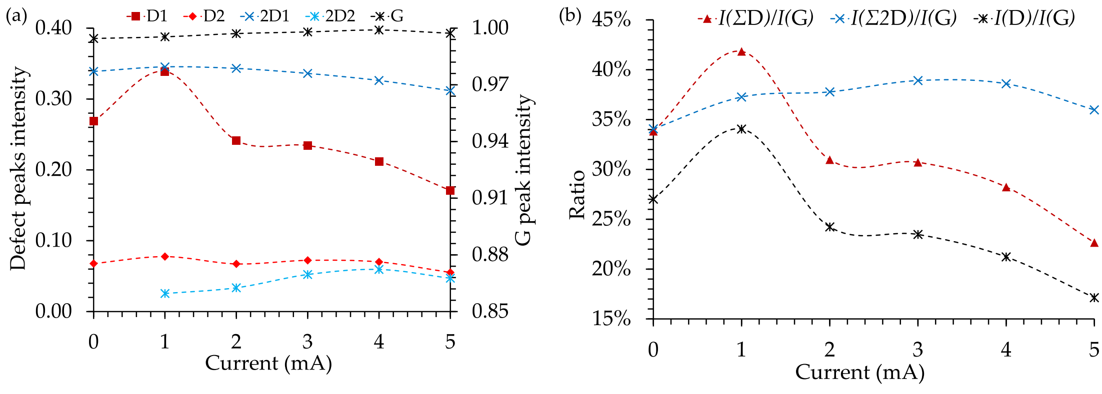

Figure 10. The changes in Raman shift (a) peaks intensity and (b) defects to graphitic intensity ratio as functions of the flowing electrical current through colloidal graphite.

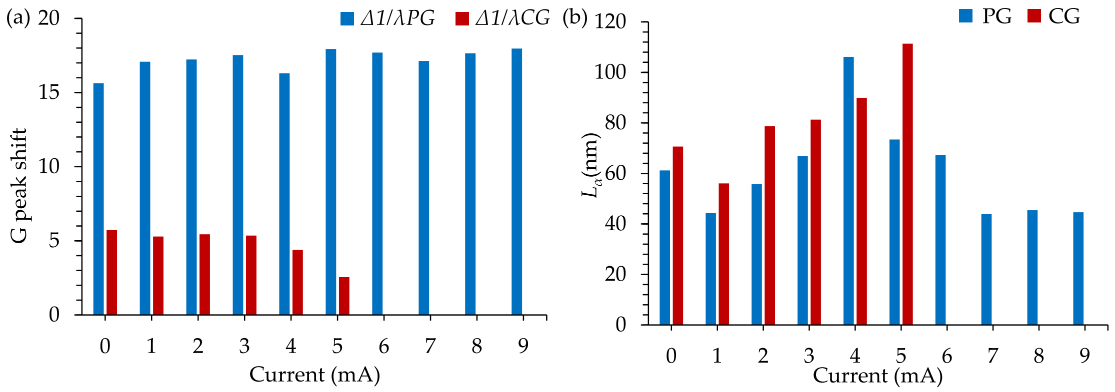

Figure 11. Statistical Interpretation of the (a) shift in G peak and (b) crystallite size for polymer graphite and colloidal graphite.

the structure stability of CGC. The complete and detailed report on the intensity ratios is included in the Supplemental table 4.

According to the behavior of the defect peaks, impurities in the polymer graphite structure caused defects related to empty vacancies, local disorder, and amorphization of the graphite flakes [20]. This affected not only the intensities of the vibration modes, but also the shift of the peaks. The shift in the case of polymer graphite was found to be much higher than in the case of colloidal graphite, as presented in figure 11(a). In addition, it fluctuated in a quasi-harmonic form as the current changes. In contrast, colloidal graphite was shifting towards an ideal graphitic peak reported at 1560 cm^{-1} [21–23]. Moreover, XPS images showed a significant contribution of silicon in the structure of PGCs, which can cause such types of defects.

Furthermore, the improvement in structure stability was followed by tracking changes in crystallite size (L_α) as found by Cançado *et al*. According to their theory, L_α is given by [24]:

$$L_\alpha(\text{nm}) = (2.4 \times 10^{-10})\lambda_l^4\left(\frac{I_D}{I_G}\right)^{-1} \tag{1}$$

where λ_l is the laser excitation wavelength. Substituting the ratios I_D/I_G together with $\lambda_l = 532$ nm, L_α was found as a function of the applied current as presented in figure 11(b). Following the behavior of the I_D/I_G ratio for each type of cathode, the values of L_α for polymer graphite fluctuated and reached their maximum value when the current was 4 mA. However, for colloidal graphite, L_α increased as the ratio I_D/I_G decreased.

Finally, the results obtained in this study prove what was found by Trnkova *et al* in [17], Navratil *et al* in [5], and Li *et al* in [15, 16] in their research on the performance of polymer graphite in electrochemistry. In their research, they showed that pencil leads that contain a polymer binding agent have improved conductivity compared to non-polymer pencil leads. However, they also showed that the conductivity is enhanced for polymer graphite pencil leads when the percentage of graphite is increased in the structure of the pencil lead. These assumptions can be verified by the relation between the plasmon-electron interaction and the existence of

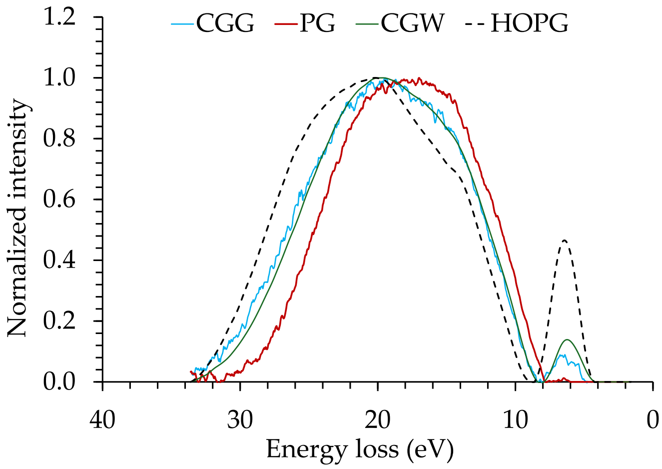

Figure 12. Reflection electron energy loss spectroscopy measurement for colloidal graphite deposited on glass (CGG), colloidal graphite deposited on tungsten (CGW), polymer graphite (PG), and high order pyrolytic graphite (HOPG).

a polymer binding agent. For this reason, REELS experiments were performed on colloidal graphite deposited on glass, colloidal graphite deposited on a metal (tungsten), polymer graphite, and high-order pyrolytic graphite (HOPG). HOPG was tested as a reference sample to check which of the cathodes will have relatively close behavior.

The results are presented in figure 12, and it shows that colloidal graphite samples followed the behavior of HOPG and they had the same first and second plasmon-electron reaction peaks. Despite that, it is clear that when glass was used as a substrate, it affected the surface conductivity of the samples. However, the spectrum of the PG showed the absence of the first plasmon-electron peak and a shift from ≈ 20 eV to ≈ 17.5 eV in the second plasmon-electron interaction peak. Thus, REELS results show another evidence that the polymer binding material in polymer graphite has a significant role in the electrical current fluctuations because of its presence within the graphite structure as a disorder defect material.

4. Conclusion

In conclusion, impurities and the presence of the polymer binding agent play a significant role in the electrical current fluctuations in polymer graphite. The results of this research compared the changes in the Raman spectroscopy spectra as the flowing electrical current is increased in polymer graphite, in addition to comparing the results with the Raman spectra of the colloidal graphite structure when deposited on glass. The findings of this study were supported by results obtained from REELS, XPS, and SEM.

Moreover, colloidal graphite showed a unique performance when deposited on an insulated substrate, which raised the interest to study its behavior when deposited on highly oxidized metallic substrates to enhance their surface conductivity in the nanoscale surface layers. This interest was raised after comparing the results of glass-graphite and tungsten-graphite REELS spectra, where it showed that colloidal graphite has behavior similar to that of HOPG when deposited on metallic surfaces.

The advantages of colloidal graphite cathodes provide a wide range of potential applications. Future work is planned to test the performance of such coatings in enhancing the conductivity of tungsten for scanning tunneling microscopy applications, mainly when the experiments are performed outside ultrahigh-vacuum environments. Moreover, future plans are considered for the glass-graphite cathodes for electochemistry applications, mainly in batteries and biosensing applications.

Acknowledgments

The research described in the paper was financially supported by the Internal Grant Agency of the Brno University of Technology, grant numbers CEITEC VUT/FEKT-J-23-8307, CEITEC VUT/FEKT-J-24-8567, and FEKT-S-23-8162.

The described research was supported by the Czech Technology Agency (FW03010504). We also acknowledge the Czech Academy of Sciences (RVO:68081731).

CzechNanoLab project LM2018110 funded by MEYS CR is gratefully acknowledged for the financial support of the measurements/sample fabrication at CEITEC Nano Research Infrastructure.

Data availability statement

The data that supports the findings is presented in the supplementary materials. The data that support the findings of this study are available upon reasonable request from the authors.

ORCID iDs

Mohammad M Allaham https://orcid.org/0000-0002-4931-0419
Samer I Daradkeh https://orcid.org/0009-0001-1937-9191
Zuzana Košelová https://orcid.org/0000-0002-1084-9935
Rashid Dallaev https://orcid.org/0000-0002-6823-5725
Dinara Sobola https://orcid.org/0000-0002-0008-5265
Alexandr Knápek https://orcid.org/0000-0003-0752-8214

References

[1] Ławrowski R, Bachmann M and Schreiner R 2022 Field emission arrays from graphite fabricated by laser micromachining *Journal of Vacuum Science & Technology* B **40** 023203
[2] Endo T, Higuchi T, Yamada Y and Sasaki M 2012 Field emission from mechanical pencil lead and graphite edges *International Vacuum Electron Sources Conference, IVESC 2012 (Monterey, CA, USA, 24-26 April 2012)* (IEEE) pp 307–8
[3] Mamidi S, Pandey A K, Pathak A D, Rao T N and Sharma C S 2021 Pencil lead powder as a cost-effective and high-performance graphite-silica composite anode for high performance lithium-ion batteries *J. Alloys Compd.* **872** 159719
[4] Knápek A, Dallaev R, Burda D, Sobola D, Allaham M M, Horáček M, Kaspar P, Matějka M and Mousa M 2020 Field emission properties of polymer graphite tips prepared by membrane electrochemical etching *Nanomaterials* **10**
[5] Navratil R, Kotzianova A, Halouzka V, Opletal T, Triskova I, Trnkova L and Hrbac J 2016 Polymer lead pencil graphite as electrode material: Voltammetric, XPS and Raman study *J. Electroanal. Chem.* **783** 152–60
[6] Annu, Sharma S, Jain R and Raja A N 2020 Review—pencil graphite electrode: an emerging sensing material *J. Electrochem. Soc.* **167** 037501
[7] Ataide V N, Arantes I V S, Mendes L F, Rocha D S, Baldo T A, Coltro W K T and Paixão T R L C 2022 Review–A pencil drawing overview: from graphite to electrochemical sensors/biosensors applications *J. Electrochem. Soc.* **169** 047524
[8] Nawi S N M, Khandaker M U, Bradley D A, Abdul Sani S F, Almugren K S and Sulieman A 2020 Polymer pencil lead graphite for in vivo radiation dosimetry *Diam. Relat. Mater.* **106** 107860
[9] Knápek A, Allaham M M, Burda D, Sobola D, Drozd M and Horáček M 2023 Explanation of the quasi-harmonic field emission behaviour observed on epoxy-coated polymer graphite cathodes *Materials Today Communications* **34** 105270
[10] Allaham M M *et al* 2024 Comprehensive analysis of charge carriers dynamics through the honeycomb structure of graphite thin films and polymer graphite with applications in cold field emission and scanning tunneling microscopy *Surfaces and Interfaces* **53** 105102
[11] Nikiel L and Jagodzinski P W 1993 Raman spectroscopic characterization of graphites: A re-evaluation of spectra/ structure correlation *Carbon* **31** 1313–7
[12] Calliari L, Fanchenko S and Filippi M 2007 Plasmon peak inhomogeneous broadening in reflection electron energy loss spectroscopy from carbon materials *Surf. Interface Anal.* **40** 814–7
[13] Filippi M and Calliari M 2006 Measuring the energy of the graphite $\pi + \sigma$ plasmon peak *Surf. Interface Anal.* **38** 595–8
[14] Lee S H, Ban J Y, Oh C-H, Park H-K and Choi S 2016 A solvent-free microbial-activated air cathode battery paper platform made with pencil-traced graphite electrodes *Sci. Rep.* **6** 28588
[15] Li X, Triskova I and Trnkova L 2023 A new experimental approach to understanding microscopic details of the electrode/electrolyte interface *Electrochim. Acta* **442** 141921
[16] Li X, Čechal J, Spanhel L, Toscani S, Martinik J, Oborilova R and Trnkova L 2024 Intriguing properties of graphite/polysiloxane composite-based pencil electrodes *Electrochim. Acta* **475** 143615
[17] Trnkova L, Triskova I, Cechal J and Farka Z 2021 Polymer pencil leads as a porous nanocomposite graphite material for electrochemical applications: the impact of chemical and thermal treatments *Electrochem. Commun.* **126** 107018
[18] Ramya A V, Manoj B and Mohan A N 2016 Extraction and characterization of wrinkled graphene nanolayers from commercial graphite *Asian J. Chem.* **28** 1031–4
[19] Kaplas T and Svirko Y P 2012 Direct deposition of semitransparent conducting pyrolytic carbon films *J. Nanophotonics* **6** 061703
[20] Ferrari A C and Robertson J 2000 Interpretation of Raman spectra of disordered and amorphous carbon *Phys. Rev.* B **61** 14095
[21] Bradley D A, Rozaila Z S, Khandaker M U, Almugren K S, Meevasana W and Abdul Sani S F 2019 Raman spectroscopy and X-ray photo-spectroscopy analysis of graphite media irradiated at low doses *Appl. Radiat. Isot.* **147** 105–12
[22] Ferrari A C 2007 Raman spectroscopy of graphene and graphite: Disorder, electron-phonon coupling, doping and nonadiabatic effects *Solid State Commun.* **143** 47–57
[23] Karamat S, Sonuşen S, Çelik Ü, Uysallı Y, Özgönül E and Oral A 2015 Synthesis of few layer single crystal graphene grains on platinum by chemical vapour deposition *Progress in Natural Science: Materials International* **25** 291–9
[24] Cançado L G, Takai K, Enoki T, Endo M, Kim Y A, Mizusaki H, Jorio A, Coelho L N, Magalhães-Paniago R and Pimenta M A 2006 General equation for the determination of the crystallite size of nanographite by Raman spectroscopy *Appl. Phys. Lett.* **88** 136106